Hindawi
Mathematical Problems in Engineering
Volume 2022, Article ID 5737738, 13 pages
https://doi.org/10.1155/2022/5737738

Research Article

Water Inrush Mechanism of Roof Induced by the Fault Weakening Effect in the Coal Mining

Qing Qiu,[1] **Lulin Zheng**,[1] **Hong Lan**,[2,3] **Wen Zhang**,[4] **Hengyi He**,[1] **Chun Zhao**,[2] **Youwen Tian**,[2] **Hao Liu**,[3] **and Ruipeng Li**[1]

[1]*College of Mining, Guizhou University, Guiyang 550025, Guizhou, China*
[2]*Longfeng Coal Mine of Guizhou Lindong Coal Industry Development Co., Ltd., Jinsha County 551800, Guizhou, China*
[3]*College of Resource and Environmental Engineering, Guizhou University, Guiyang 550025, Guizhou, China*
[4]*College of Construction Engineering, Jilin University, Changchun 130026, Jilin, China*

Correspondence should be addressed to Lulin Zheng; llzheng@gzu.edu.cn

Received 29 June 2022; Accepted 25 July 2022; Published 19 September 2022

Academic Editor: Fuqiang Ren

The northern Guizhou coalfield exhibits complex geological conditions and well-developed structures. Hard rock formations are damaged by faults, causing frequent water inrush accidents. To study the damaging effect of faults on roof key strata and the mechanism of water inrush accidents, this paper chose the 5914 coal mining faces of the Longfeng coal mine as the engineering background, determined the water inrush source and key strata through field investigation, hydrochemical analysis, and theoretical calculation, and used RFPA-flow numerical simulation software to simulate the hydraulic coupling effect. The characteristics of the shear stress, damage degree, and hydraulic gradient were analyzed, and finally, the high-density electrical method was employed for simulation verification. The results indicated that the key stratum can control water inrush, but under the influence of faults, the roof forms multiple separation layers, and several sudden increases in displacement occur (the sudden jump phenomenon). A stress concentration area is formed in the head-end tunnel through the fault, and the number of AE events increased to 1150. The water-force gradient exhibits a uniform local large-scale evolution process, and finally, the height of the water-conducting fracture reaches 60 m through the aquifer. This height is 3 times that without fault influence. The numerical simulation results are consistent with the theoretical calculation and field analysis results, which verifies that the fault imposes a highly significant weakening effect on the key stratum, providing data support for later engineering.

1. Introduction

As the third largest coal field in Guizhou, China, the northern Guizhou coalfield is rich in coal resources, but this coalfield is located in a unique tectonic location and exhibits a complex regional geological structure, including concealed structures and karst development; coupled with the influence of the Yanshan and Himalayan movements, large-scale faults and folds were formed [1], causing the geological structure and hydrogeological conditions in the northern Guizhou coalfield to be highly complex and the types of water hazards to be varied. In particular, this coalfield is seriously impacted by karst water in roof strata [2, 3]. On August 21, 2019, the Longfeng coal mine of the Guizhou Lindong Group Mining Co., Ltd., is located in the northern Guizhou coalfield. Due to the influence of hidden faults, water inrush caused by karst cave water in the roof of the coal seam resulted in 2 deaths and a direct economic loss of more than 5 million yuan. The investigation of the accident shows that there is a fault during the excavation of the working face on June 19, and the water from goaf roof at the outlet under the mining face increased. Then, during July 22 to August 6, the roof burst several times, and on August 21, gangue and water from the roof suddenly poured into the working face, causing the accident. Nowadays, many underground projects involve water-force coupling [4, 5], and for mine water damage, the water source and water inrush channel are highly hidden. Therefore, it is necessary to

clarify the occurrence conditions of the water inrush source, action mechanism of the geological structure in regard to the water-conducting fracture, especially to study the coupling relationship between faults and the roof lithology under water-force action, and action characteristics and evolution pattern of the roof water-conducting fracture zone.

Scholars have performed much work regarding the prevention of karst water damage and the mechanism of water inrush. Based on mechanics theory, research has been conducted to determine the failure pattern of water-conducting fracture zones. Among these studies, the most representative theories include the three-zone theory [6], four-zone model [7], and key stratum theory [8]. According to the key stratum theory, when there are multiple hard strata among the overlying strata in the stope, these strata control all or part of rock mass activities, which are referred to as key strata. Based on this theory, most experts have conducted in-depth studies of filling mining, co-mining of coal and gas, prediction of water-conducting fracture zones, and other aspects [9–11]. The stress transfer path and stress distribution near key strata exhibit notable characteristics in the coal mining process [12], and the difference in the fracture deformation zone of the key stratum affects the roof waterproofing performance [13]. In addition, scholars acknowledge that the key stratum provides a good control effect on the formation of water-conducting fracture zones [14], the failure pattern of overburden rock [15], and water inrush from the mine roof and floor [16]. However, as a specific geological structure, faults are widely found in the northern Guizhou coalfield [17]. The faults destroy the continuity of coal seam and roof strata, enlarge the breaking range of surrounding rock, and seriously threaten the safe production of mine. According to statistics, 80% of water inrush accidents are related to faults [18, 19]. Faults not only control the structural morphology of water-bearing systems but also control the dynamic conditions of groundwater [20]. A lot of studies have been done on the relationship between fracture evolution and rock fracture, and it is believed that the existence of fracture seriously affects rock fracture behavior [21, 22]. When the tunnel face occurs close to a fault, the fracture activation frequency of the surrounding rock increases, and the fault can penetrate the hard waterproof layer, resulting in water inrush accidents between the surrounding rock and aquifer [23].

With the continuous development of computer technology, numerical simulation has become an important method to research the failure mechanism of roof overlaying rock and the mechanism of water inrush. The commonly used numerical simulation software programs include RFPA, UDEC, and FLAC3D. Among the above software packages, RFPA numerical simulation software is based on finite element and meso-damage statistics theory, and fully considers the heterogeneity of rock material, the randomness of defect distribution, and the influence of water on rock mass fracture development which makes it to be widely used in the study of rock fracture, roof and floor rock and failure laws, and water inrush from roof and floor of coal seam. Liu et al. [24, 25] combined the RFPA and fractal theory to study the fracture evolution characteristics of sandstone and single joint sandstone. Ma et al. [26] applied RFPA-2D to study the fracture behavior of rock mass near faults. Yu et al. [27] applied the rock fracture process analysis system RFPA-2D to analyze the dynamic development process of overburden rock failure under the influence of mining. Zhang et al. [28] simulated the hydraulic fracturing and studied the evolution law of crack propagation and acoustic emission by RFPA-flow. Wang et al. [29] used RFPA-flow to study the influence of confining pressure and pore pressure crack propagation and permeability of rock mass under uniaxial compression and, on this basis, analyzed the formation mechanism of floor water inburst channel.

Previous studies have studied the theoretical research on mine water inrush by studying the movement, deformation, and failure of roof overburden under the influence of faults and the development law of water-conducting fracture zone, but the formation of water inrush accidents involves a very complex process. Structural damage, control of key strata, and water-rock interactions constitute some of the multiple factors leading to roof water damage, and research on this aspect is scarce in the northern Guizhou coalfield. Therefore, it is necessary to select typical coal mines in the northern Guizhou coalfield as examples to study the weakening effect of faults on key strata and the mechanism of mine water inrush under the action of water and rock.

2. Engineering Background

In the Longfeng coal mining area, the strata are gently sloping, and the geological structure is simple, but a concealed structure is developed. During the exploration period, 11 hidden faults were exposed through drilling, and more than 100 small hidden faults were revealed. Coal seams in the area mainly occur in the Upper Permian Longtan Formation (P_3l), and the average thickness of the Longtan Formation reaches approximately 98 m, belonging to marine and continental cross-deposits. At present, the main mining target is the 9# coal seam. The direct roof of the 9# coal seam is silty mudstone, and the upper part comprises siltstone or fine sandstone. The direct floor is argillaceous siltstone, while silty mudstone and siltstone occur locally. The overlying water-filled aquifers include the Yulongshan Member of the Triassic Yelang Formation (T_1y^2) and the Upper Permian Changxing Formation (P_3c). The vertical distance between coal seam no. 9 and the bottom boundary of the Changxing Formation limestone karst water aquifers is 34.98 m, and the thickness of the Changxing Formation aquifers ranges from 24.13 to 35.50 m, with an average thickness of 29.44 m. In the absence of atmospheric water supplementation, the water level of the aquifer remains stable at approximately 50 m. The roof lithology of 5914 working face is mainly determined according to borehole ZK2-5 and drilling data of advanced geological exploration. The rock formation combination and rock parameters are shown in Figure 1.

The mining face of the Longfeng coal mine adopts the backwall-type mining method, and the roof mining method is adopted to manage the roof. Meanwhile, the 4# and 5# coal seams above the 9# have not been mined. The roof is stable and does not easily collapse, which plays an obvious controlling role on rock stratum activities, and the key stratum

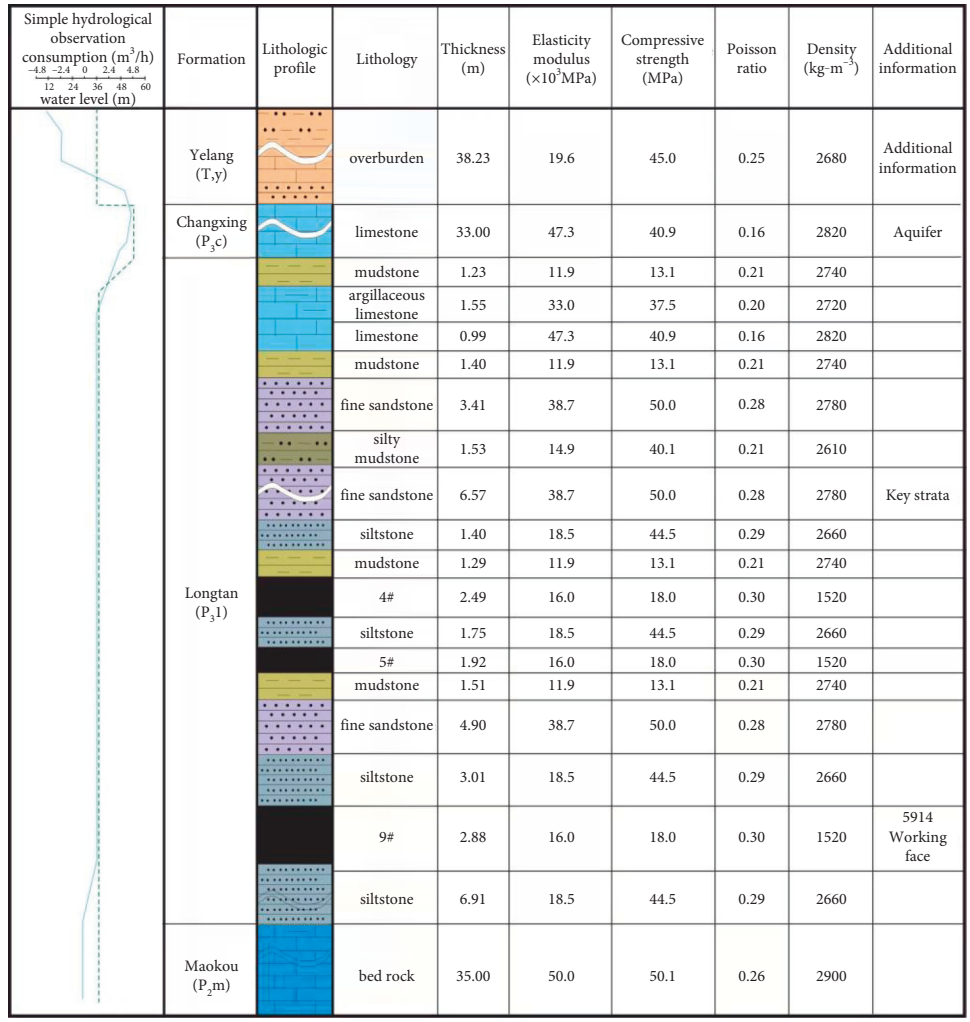

Formation	Lithologic profile	Lithology	Thickness (m)	Elasticity modulus ($\times 10^3$MPa)	Compressive strength (MPa)	Poisson ratio	Density (kg·m^{-3})	Additional information
Yelang (T,y)		overburden	38.23	19.6	45.0	0.25	2680	Additional information
Changxing (P_3c)		limestone	33.00	47.3	40.9	0.16	2820	Aquifer
Longtan (P_3l)		mudstone	1.23	11.9	13.1	0.21	2740	
		argillaceous limestone	1.55	33.0	37.5	0.20	2720	
		limestone	0.99	47.3	40.9	0.16	2820	
		mudstone	1.40	11.9	13.1	0.21	2740	
		fine sandstone	3.41	38.7	50.0	0.28	2780	
		silty mudstone	1.53	14.9	40.1	0.21	2610	
		fine sandstone	6.57	38.7	50.0	0.28	2780	Key strata
		siltstone	1.40	18.5	44.5	0.29	2660	
		mudstone	1.29	11.9	13.1	0.21	2740	
		4#	2.49	16.0	18.0	0.30	1520	
		siltstone	1.75	18.5	44.5	0.29	2660	
		5#	1.92	16.0	18.0	0.30	1520	
		mudstone	1.51	11.9	13.1	0.21	2740	
		fine sandstone	4.90	38.7	50.0	0.28	2780	
		siltstone	3.01	18.5	44.5	0.29	2660	
		9#	2.88	16.0	18.0	0.30	1520	5914 Working face
		siltstone	6.91	18.5	44.5	0.29	2660	
Maokou (P_2m)		bed rock	35.00	50.0	50.1	0.26	2900	

Figure 1: Columnar and rock formation parameter map of the ZK2-5 borehole in the Longfeng coal mine.

features are obvious. However, during the advancement of the 5914 working face of the 9# coal seam, several water gushing and slurry collapse events occurred in the roof, and the water outlet of goaf roof under mining face increased on June 19, 2019. The subsequent investigation determined that there occurred an east-west fault fracture with a dip angle of 43° and a length of 12 m above the roof in this accident. This fault is located below the key stratum, which resulted in a connection between the aquifer and C9 coal seam, thus causing the aforementioned water inrush accident. A field geological survey found that there were several similar concealed faults east of the 5914 mining face, and small faults were connected with the F1 fault traversing the northern and southern parts of the mining area, which became a potential risk factor in the later advancement process. An overview of the 5914 working face and the accident site is shown in Figure 2.

3. Determination of Roof Water Damage Source and Key Strata

3.1. Determination of Water Hazard Sources. To further determine the source of water damage, before the arrival of the heavy rainfall period (thus excluding the influence of external water sources on the water sample composition under the action of precipitation), outlet water point S-1 below the working face, water interception point S-2 in a 300 m borehole in the 5914 working face, and water seepage point S-3 at the no. 11 support (the water intake point is shown in Figure 2) were considered, and water samples of the overlying aquifer were analyzed to determine the water quality. The results are listed in Table 1.

The mass concentration of Ca^{2+} in the gushing water at S-1, S-2 and S-3 ranged from 3.55 to 48.42 mg·L^{-1}, and the mass concentration of $K^+ + Na^+$ ranged from 101.06 to 129.06 mg·L^{-1}. Moreover, the hydrochemical type of the S-1 and S-3 samples is HCO_3·SO_4-Mg·K + Na, and the hydrochemical type of the S-2 sample is HCO_3·SO_4-Mg·K + Na·Ca. Comparison reveals that the ion concentration in the water samples is similar to that in the Changxing Formation aquifer, and the water chemical type is consistent, indicating that water inrush in the 5914 mining face stems from the Permian Changxing Formation limestone karst water aquifer in the roof.

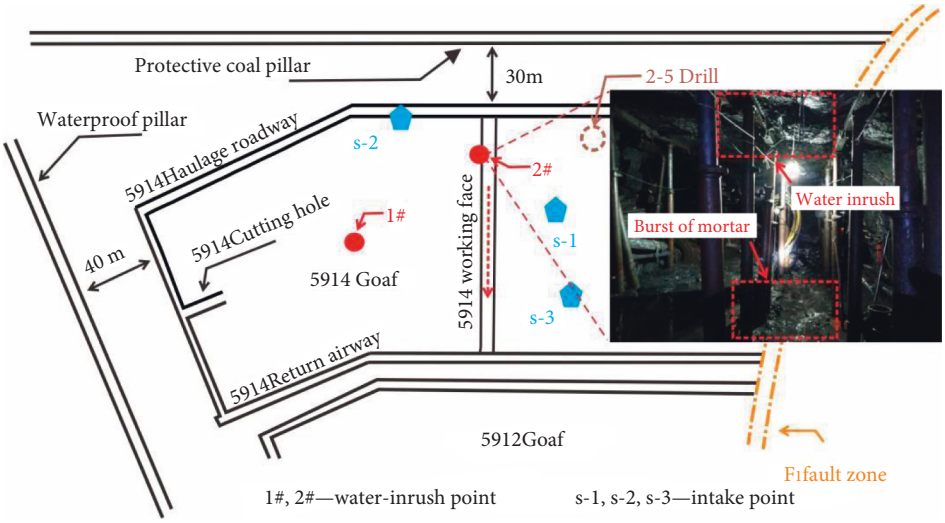

Figure 2: Overview of the working face and accident site.

Table 1: Water quality analysis results.

Sample	pH	Mass concentration of each ion/(mg·L^{-1})							Type of water
		Ca^{2+}	Mg^{2+}	$K^+ + Na^+$	Cl^-	SO_4^{2-}	HCO_3^-	NO_3^-	
T_1y-1	7.61	77.21	2.98	10.02	13.12	33.75	286.48	4.80	HCO_3-Ca
T_1y-2	7.80	70.20	3.68	31.61	10.35	51.04	227.53	6.00	HCO_3-Ca
P_3c-1	7.70	17.96	67.86	271.22	13.93	264.25	273.17	3.60	HCO_3·SO_4-Mg·K + Na
P_3c-2	8.30	25.48	63.65	143.61	15.42	267.91	199.04	2.40	HCO_3·SO_4-Mg·K + Na
S-1	7.94	10.65	53.20	129.06	20.49	271.24	248.71	2.80	HCO_3·SO_4-Mg·K + Na
S-2	8.34	48.42	68.74	101.06	18.01	294.7	246.76	2.80	HCO_3·SO_4-Mg·K + Na·Ca
S-3	7.87	3.55	50.15	115.98	28.58	196.73	216.37	2.00	HCO_3·SO_4-Mg·K + Na

3.2. Determination of the Key Stratum. Because of the different properties of coal and rock, the breaking patterns of the rock strata are different from those of the fully mechanized mining face. The overall weight of the overburden is borne by hard and thick rock strata, which can control the roof collapse distance and are collectively denoted as the key stratum [8]. The position of the key stratum is determined according to equation (1), and a corresponding calculation model is shown in Figure 3.

If the 1 to m hard strata are deformed but the $m+1$ stratum is not deformed, the latter hard stratum then constitutes the second layer. Since the strata are deformed from the first layer to the m-th layer, the load on the hard strata in the first layer [30] is

$$q_{(m)1} = \frac{E_1 h_1^3 \sum_{i=1}^{m} h_i r_i}{\sum_{i=1}^{m} E_i h_1^3}, \tag{1}$$

where $q_{(m)1}$ is the load of the m-th rock layer on the hard rock layer; h_i is the thickness of layer i, m; r_i is the bulk density of rock layer i, MN/m^3; and E_i is the elastic modulus of rock layer i, GPa.

It is assumed that the $m+1$ layer is another hard layer. Since its deflection is smaller than that of the lower layer, the $m+1$ layer does not synchronously deform with the lower layer. Therefore, the following applies:

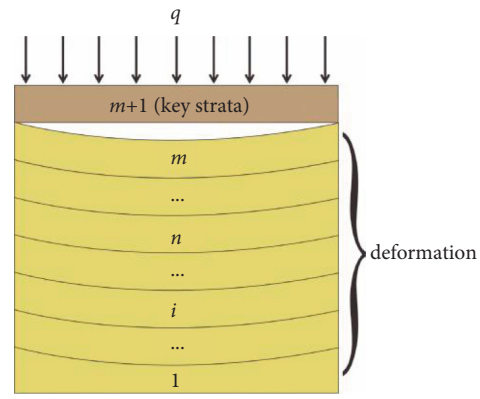

Figure 3: Key stratum load model.

$$q_{(m+l)l} < q_{(m)l}. \tag{2}$$

Substituting equations (1) into (2), an evaluation equation of the position of the hard rock layers can be obtained after simplification as [31]

$$E_{m+1} h_{m+1}^2 \sum_{i=1}^{m} h_i r_i r_{m+1} \sum_{i=1}^{m} E_i h_1^3. \tag{3}$$

In actual assessment, the calculation starts from the first layer of the working surface and proceeds upward layer by

layer. When equation (3) is satisfied, the corresponding rock layer is the first hard rock layer. The calculation process is continued upward until the top hard layer can be identified, after which the calculation is stopped. The specific location of hard and soft rock layers can be ensured through the above calculation process.

Based on geological drilling data of borehole ZK2-5 (Figure 1) and combined with the above derivation equation, it is concluded that the key stratum of the 5914 working face is a 6.57-m-thick fine sandstone layer (Figure 1).

4. Numerical Simulation of Roof Water Gushing under the Weakening Effect of a Fault on the Key Stratum

4.1. Model Calculation Method. RFPA^{2D}-flow is a numerical analysis system based on finite element theory, which can fully consider nonlinear, nonuniform, and anisotropic changes in rock strata and karst water in the process of coal seam mining and can better analyze the evolution process of roof water damage under the coupling action of seepage and stress. The mechanical parameters of the RFPA material model of the meso-structure are based on laboratory test results, the karst water aquifer follows Biot consolidation theory, and the material stress-permeability coefficient relationship can be described by a negative exponential equation [32]:

$$Kf = K_0 e^{-b\sigma}, \tag{4}$$

where K_0 is the initial permeability coefficient, σ is the normal stress, and b is a coupling parameter.

The seepage behavior of fluid varies with the damage degree of the rock mass. Therefore, the coupling effect of seepage, stress, and damage must be considered to accurately reflect the real conditions through numerical simulation. The basic equation of fluid-solid seepage coupling is as follows:

The equilibrium equation is

$$\frac{\partial \sigma_{ij}}{\partial x_{ij}} + \rho X_j = 0, \quad (i, j = 1, 2, 3). \tag{5}$$

The geometric equation is

$$\varepsilon_{ij} = \frac{1}{2}\left(u_{i,j} + u_{j,i}\right), \quad \varepsilon_v = \varepsilon_{11} + \varepsilon_{22} + \varepsilon_{33}. \tag{6}$$

The seepage equation is

$$K\nabla^2 p = \frac{1}{Q}\frac{\partial p}{\partial t} - \alpha\frac{\partial \varepsilon_v}{\partial t}. \tag{7}$$

The seepage-stress coupling model is

$$K(\sigma, p) = \xi K_0 e^{-\beta\left(\left(\sigma_{ii}/3\right) - \alpha p\right)}, \tag{8}$$

where ρ is the density, σ_{ij} is the sum of the normal stresses, εv and ε_{ii} are the volumetric strain and normal strain, respectively, δ is the Kronecker constant, Q is Biot's constant, G and λ are the shear modulus and Ramet coefficient, respectively, ∇^2 is the Laplace operator, P is the pore water pressure, and ξ, α, and β are the permeability coefficient jump ratio, pore water pressure coefficient, and coupling coefficient (stress-sensitive factor), respectively. The values are determined via experiments and exhibit certain changes between different states.

Numerous experimental results have demonstrated that the permeability coefficient is not only a function of stress but also a function of the evolution of stress-induced damage and rupture. According to the coupling equation of seepage and damage, when the stress state or strain state of a given element meets a certain damage threshold, the element is damaged, and the elastic modulus of the damaged element is [33]

$$E = (1 - D)E_0, \tag{9}$$

where D is the damage variable and E and E_0 are the elastic modules of the damaged and lossless elements, respectively.

Choosing the uniaxial tensile constitutive model as an example, the seepage-damage coupling equation of the element is expressed below [34]:

When the element strength reaches the tensile strength f_t damage threshold, the following applies:

$$\sigma_3 \le -f_t. \tag{10}$$

The damage variable is

$$D = \begin{cases} 0, \varepsilon_{t0} \le \varepsilon, \\ 1 - \dfrac{f_{tr}}{E_0 \varepsilon}, \varepsilon_{tu} \le \varepsilon < \varepsilon_0, \\ 1, \varepsilon \le \varepsilon_{tu}, \end{cases} \tag{11}$$

where f_{tr} is the residual strength and ε_{t0} and ε_{tu} are the maximum and ultimate tensile strains, respectively.

The unit permeability coefficient is

$$K = \begin{cases} K_0 e^{-\beta\left(\sigma_3 - \alpha p\right)}, D = 0 \\ \xi K_0 e^{-\beta\left(\sigma_3 - \alpha p\right)}, 0 \le \varepsilon < 1 \\ \xi' K_0 e^{-\beta\left(\sigma_3 - p\right)}, D = 1 \end{cases} \tag{12}$$

Similarly, the permeability-damage coupling equation of the uniaxial compression unit can be obtained, as shown in Figure 4.

4.2. Model Settings. The evolution process of roof water gushing under the weakening action of faults is considered. Based on the actual working conditions of Longfeng coal mine, the size of the model was set to 150 m × 300 m, and 300 × 600 grid cells were divided. An equivalent load of 1 MPa of the overburden layer and a 50 m water head (reflecting the water pressure of the Changxing Formation aquifer) were applied to the upper part of the model. According to the revealed faults, the dip angle of the fault is 45° and the length was set 12 m. Because only the evolution

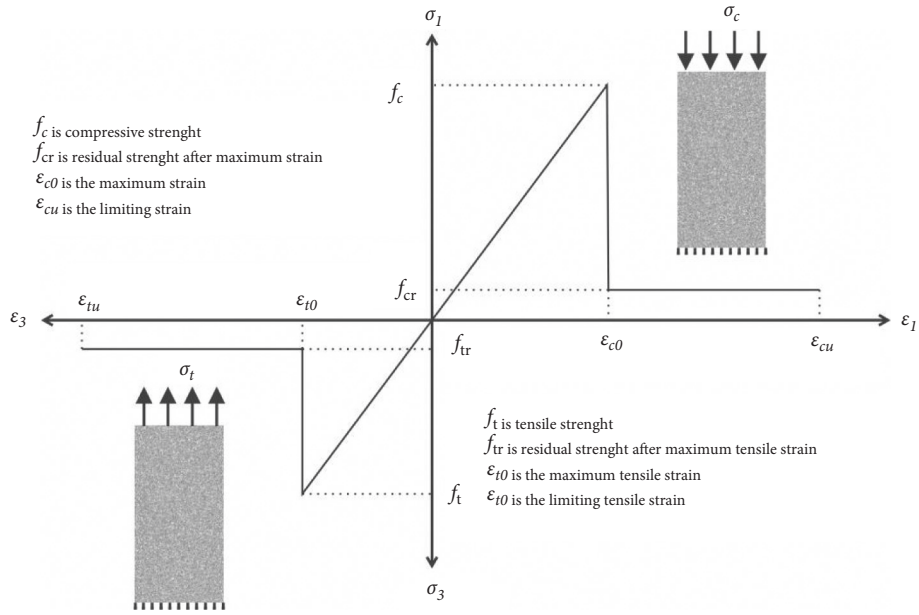

Figure 4: Meso-element constitutive model under uniaxial compression and tension.

process of roof water inrush under the influence of faults on the weakening of key layers was analyzed, the horizontal displacement of both sides of the model boundary and vertical displacement of the bottom surface were constrained, and fault parameters were set based on the weakening element method. The plane strain model was adopted for calculation. Due to the boundary effect, 50 m coal pillars were reserved on the left side of the model, and continuous excavation was carried out starting from the second step, with 10 m excavated at each step. The simplification of the established numerical calculation model is shown in Figure 5, and the attributes and physical and mechanical parameters of the rock strata in the model are shown in Figure 1.

4.3. Evolution of the Shear Stress Field in the Surrounding Rock of the Roof. Since a rock mass occurring at the intersection of the maximum and minimum principal stresses is highly prone to failure and the failure form mainly involves shear failure [35], only shear stress characteristics were analyzed. Four measuring points in the roof of the coal seam were set for y-direction displacement monitoring at the 60 m level (without fault influence), 20 m level (with minor fault influence), 10 m level (affected by the fault), and 0 m level (fault layer). The monitoring results are shown in Figure 6(d). As shown in Figure 6(a), the roof of the coal seam is affected by mining, and the maximum principal stress is distributed at the junction of soft and hard coal rock layers and the face of the mined-out area. With eastward advancement of mining, the stress in the roof shear stress concentration area uniformly increases, deformation of the surrounding rock continues to develop, and the overall failure range increases by a small margin. As shown in Figure 6(b), fault activation is clearly observed. A stress concentration distribution area emerges in both the upper and lower areas of the fault, and the stress concentration area is connected to the working face. Fractures become connected with the fault and vertically develop toward the lower part of the key stratum. Subsequently, the activated area of the fault rapidly increases, and the surrounding rock fails and releases pressure, leading to expansion of the unconsolidated zone to greater depths. The response of the separation zone in the upper part of the fault is notable, which leads to the highest transverse development speed of the fracture in the upper part of the fault, and a longitudinal fracture gradually develops through the aquifer. With intensification of microfracture events, the seepage and scouring effects of karst water in the aquifers on the fracture result in deterioration of the mechanical properties of the fault, and the fracture rapidly penetrates through the working face and fault. As shown in Figure 6(c), the working face fissure eventually becomes connected with the fault fissure, the fissure in the upper part of the fault suddenly develops upward along with the fracture in the key stratum [36], and the phenomenon of a sudden jump occurs. The surrounding rock is increasingly damaged to form a water-conducting fracture zone, and the development height of the water-conducting fracture zone reaches approximately 55 m. Compared to the fault-free roof during the early mining period, only one separation zone is formed in the early goaf without fault influence, and the height of the fracture zone reaches approximately 25 m, which is consistent with the height of 24.68 m of the fracture zone obtained based on the Exploration Specification of Hydrogeology and Engineering Geology in mining areas (GB/T 12719-2021).

$$H = \frac{100 \Sigma M}{3.1 \Sigma M + 5.0} \pm 4.0, \tag{13}$$

where M is thickness of the coal seam, m (2.88 m); combined with the analysis results shown in Figure 6(d), it is found that the displacement of the measuring point at the 60 m level

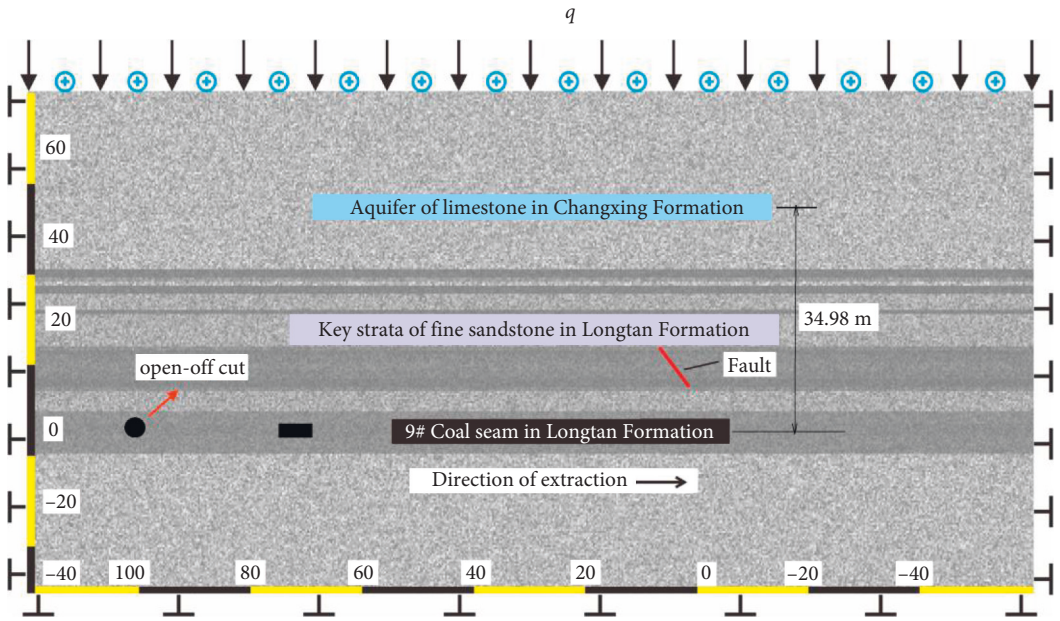

Figure 5: Numerical calculation model.

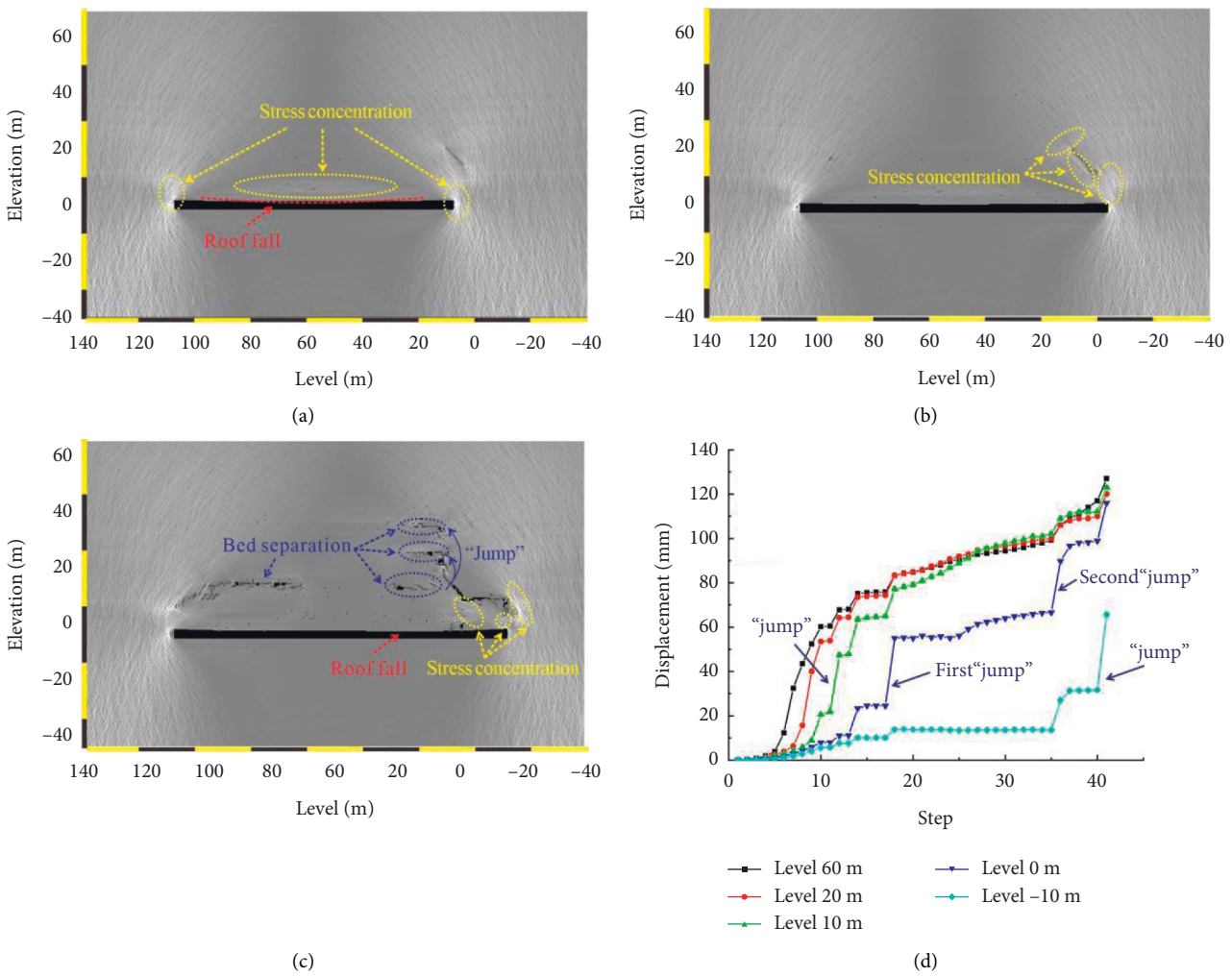

Figure 6: Shear stress cloud map and roof displacement analysis.

steadily increases throughout the whole process, and the key stratum provides a good control effect. Horizontal displacement of the 10 m roof measuring point occurred several times under low and continuous instability, corresponding to the process in which the stress in the footwall of the fault and upper and lower parts was gradually released at the early stage of mining, fault cracks were penetrated, and the key stratum was locally damaged. The horizontal displacement of the 0 m measuring point exhibited two clear sudden changes, which were caused by the weakening control effect of the failure of key stratum and the sudden jump phenomenon attributed to the penetration of the roof water-conducting fissure zone. After the sudden jump phenomenon occurred, a high-stress concentration area was formed in the head at −10 m. After 40 steps, the displacement significantly changed. The roof closer to the fault was very prone to caving, which imposed the greatest influence on mining caving at the later stage.

Therefore, due to the presence of the key stratum, the deformation and failure of the roof are well controlled, and the development of cracks in the strata is relatively smooth. Meanwhile, the water-conducting fracture zone could not be effectively connected, which could effectively reduce the risk of roof collapse, thus reducing the possible of mine water hazard. Under the influence of faults, the roof displacement of the key stratum can vary, and three separation zones can be rapidly formed above the key stratum. The integrity of roof strata is destroyed, cracks develop, and the height of the developed water-conducting fracture is 2-3 times that of the water-conducting fracture without the influence of faults, which accelerates the formation of water inrush channels and increases the risk of a sudden influx of water from aquifers into the working face. What's more, the closer the key stratum occurs to the fault, the larger the area of the separation zone is and the higher the risk of roof collapse is. The presence of faults significantly weakens the strength of the key stratum, greatly reduces the control effect of the key stratum on the water-conducting fracture zone, increases the damage range of the roof both horizontally and longitudinally, results in the roof most obviously sinking near the fault layer, and forms a high-stress area in the unmined roof, which creates concealed conditions for water inrush accidents at the later stage.

4.4. Damage and Failure Characteristics of the Surrounding Rock of the Roof Fault. The acoustic emission (AE) technique is an effective method to measure the deformation and failure of rock masses, so as to effectively reflect the failure process of coal roof. In the AE event diagram, the red unit indicates tensile damage, the white unit indicates compression damage, and the black unit indicates cumulative AE damage. As shown in Figure 7(a), when the working face occurs far from the fault, the roof of the goaf is not damaged, and successive AE events of compressive and tensile failure occur uniformly. As the working face was advanced, roof delamination damage was observed, roof pressure damage reduction occurred due to the overburden, and the AE events mainly indicated tensile damage. In the process of local damage to the surrounding rock, acoustic emission events were continuously developed in the deep surrounding rock, the AE event increment under excavation was less than 30, and the AE accumulative curve smoothly increased throughout the process. As shown in Figure 7(b), when the working face was advanced beneath the fault, the number of AE events in the fault increased to 52, and the single-step AE energy reached 156 J. Due to the insufficient bearing capacity of the fault itself, AE events mainly increased within the fault, tensile failure events largely occurred, and a small number of compressive failure events emerged at both ends of the fault. As shown in Figure 7(e), the upper part of the fault is controlled by the key stratum, and energy release is inhibited. The single-step AE energy is reduced to 86 J, AE events slowly accumulate, and the cumulative AE curve is relatively flat. With progression of the mining process, detachment occurs beneath the key stratum. When the energy accumulated in the upper part of the fault reaches a certain value, energy is first released through detachment, and AE events tend to develop toward detachment. Since the key stratum is not significantly damaged, AE events are longitudinally prevented from penetrating into the surrounding rock, and only sporadic AE events occur at the depth of the surrounding rock. As the stress in the surrounding rock at the bottom of the fault changes, AE events continue to accumulate and laterally expand along the working face. As shown in Figure 7(c), after AE events at the bottom of the fault were extended laterally across a certain distance, these AE events changed direction and followed longitudinal mining surface extension. Affected by the fault, when the working face passed beyond 20 m of the fault (Figure 7(d)), a large area of damage occurred in the key stratum, the number of AE events rapidly surged to 1530, thereby rapidly expanding toward the aquifer, and energy was concentrated in the interface area of the rock strata. However, the goaf is only affected by mining at the early stage, and the key stratum imposes a suitable control effect. Only an AE accumulation zone is formed below the key stratum, and a few AE events are distributed in the deep surrounding rock at the 0 m level. Fault activation exerts a weakening effect on the surrounding rock, which greatly increases the possibility of the formation of a water-conducting fracture zone.

4.5. Seepage Field Evolution of the Surrounding Rock in the Roof. The simulation results of the hydraulic gradient were analyzed (Figure 8). Under the influence of mining, the roof at the center of the goaf collapsed, along with the generation of scattered damage units, the hydraulic gradient curve expanded toward the roof in the middle of the goaf, but the key stratum exerted a satisfactory control effect on fracture development, and the overall hydraulic gradient curve was characterized by a small amplitude and uniform downward extension. When roof damage occurs, as shown in Figure 8(b), the water gradient curve continues below the scattered distribution of the failure unit, the hydraulic gradient curve is relatively smooth but now continues below the heading toward the fault, i.e., fault activation occurs, and

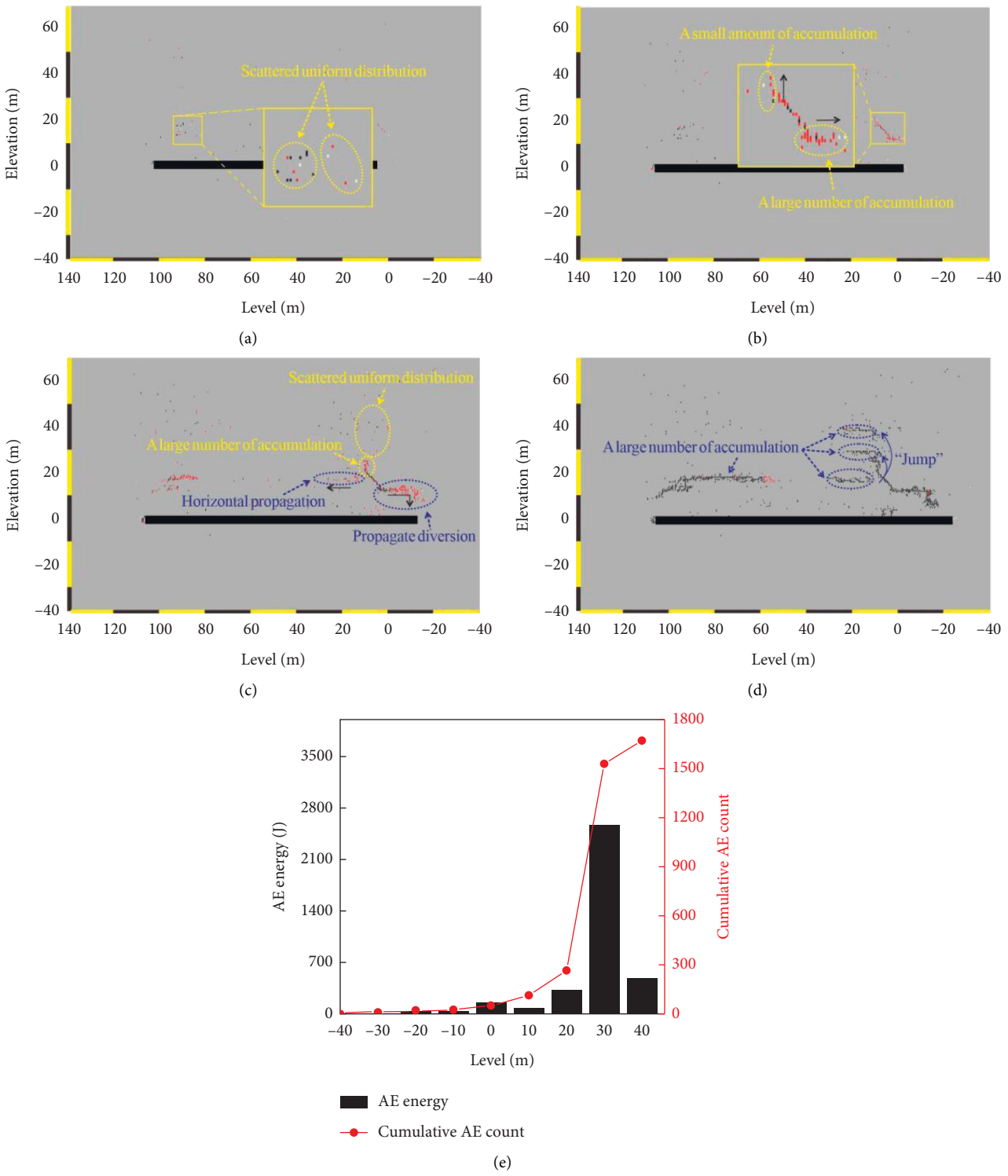

Figure 7: Analysis of the observed AE phenomena.

the hydraulic gradient curve changes along the direction of the fault, suggesting that fault activation seriously affects the distribution of the seepage field in the surrounding rock. At 10 m across the fault (Figure 8(c)), a wide range of fracture zones is formed in front and at the rear of the goaf. Through comparison of the front and rear of the goaf, it can be found that although the roof is significantly damaged, the front goaf experiences uniform change, while the rear goaf occurs under the influence of the fault. Moreover, the key stratum is damaged, and a water-conducting fracture zone is rapidly formed. The seepage gradient in the rock sharply increases, the water-conducting fracture zone becomes connected with the aquifer and working face, a seepage path is established, seepage fluid softens the rock mass around the fracture, and

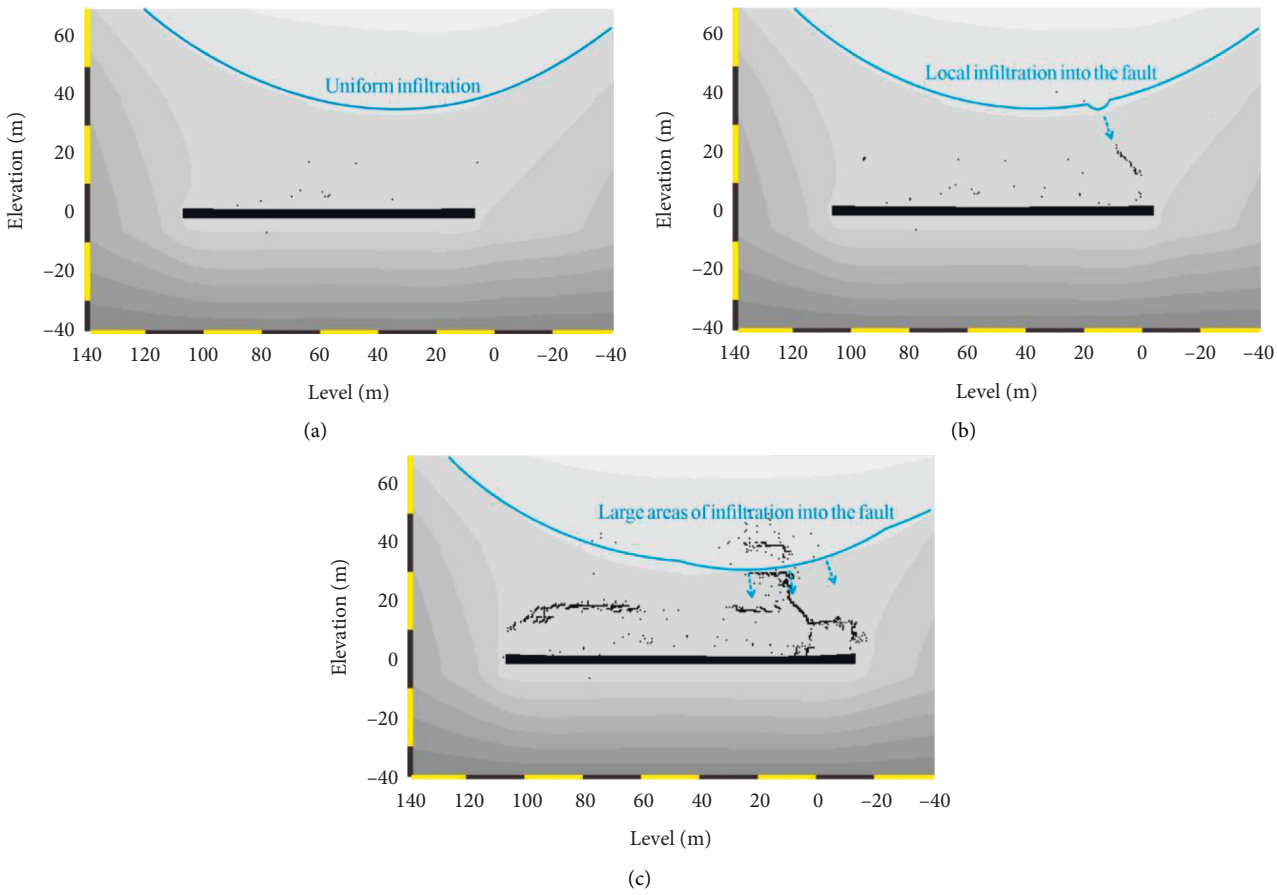

Figure 8: Diagram of hydraulic gradient evolution.

a water inrush accident occurs. In addition, the fault causes the roof in the eastern mining area to form a high-water pressure area, which reduces the security of later production.

5. Measurement of the Water-Conducting Fracture Zone and Analysis of Water Inflow in the Working Face

The high-density electrical method combined with geological data retrieved from the ZK2-5 borehole column chart was used to carry out transverse and longitudinal geophysical projections. The geophysical interpretation results are shown in Figure 9.

The above geophysical images show that the fracture zone in the mining area is irregularly developed, and concealed karst water may be widely distributed. A low-resistance zone is distributed sporadically from 0–640 m along the material detection line, which mainly involves a fissure in the Yelang Formation karst aquifer and is speculated to be a local fissure attributed to caving of the goaf roof at the early stage. At the position of the survey line from 631–1000 m, there is a strip-shaped low-resistivity anomaly, which is a fracture in the Changxing Formation aquifer. At the location of the water gushing accident in the 800 m working face, there occurs a funnel-shaped low-resistivity area, and the lower part of the low-resistivity area tends to be connected with the coal seam, which is speculated to be the water-conducting fracture zone in the working face and Changxing Formation aquifer. By analyzing the 600–900 m position in the mining area of the working face, it can be found that when the working face occurs 600–750 m from the fault, the resistance value does not change significantly, and there are no numerous fractures. The key stratum suitably controls fracture expansion. When the working face is located near 800 m (below the fault), the fissure rapidly expands, and a fissure zone is formed within a large area, generating a large funnel-shaped low-resistance area. The regional vertical distance is approximately 60 m and is tilted toward the east. This indicates that after the working face passes through the fault, the fault continuously influences the surrounding rock fissures, and stress concentration increases the extension range of the surrounding rock fissures behind the fault.

According to Figure 10, when the working face occurred 50 m from the fault on May 18, 2019, the water outflow remained stable, and the water inflow reached approximately 40 m^3/h. On June 19, the mining face passed the fault by 10 m, and a large amount of water gushing suddenly occurred in the roof of the goaf, with the water amount reaching approximately 240 m^3/h (i.e., the 1# water inrush point). To ensure the safety of the working face, slow manual advancement should occur. From July 22 to August 6, 30 m

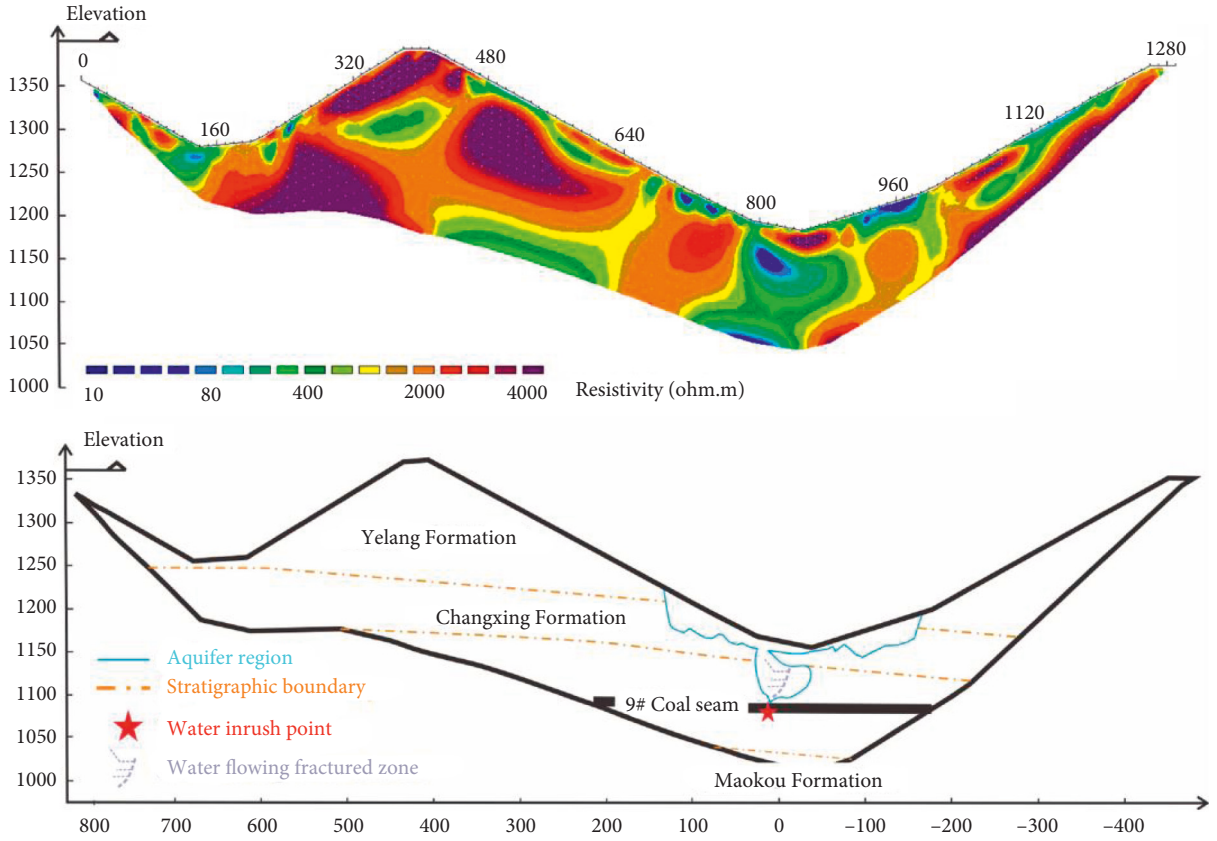

Figure 9: Image of the resistivity formation profile.

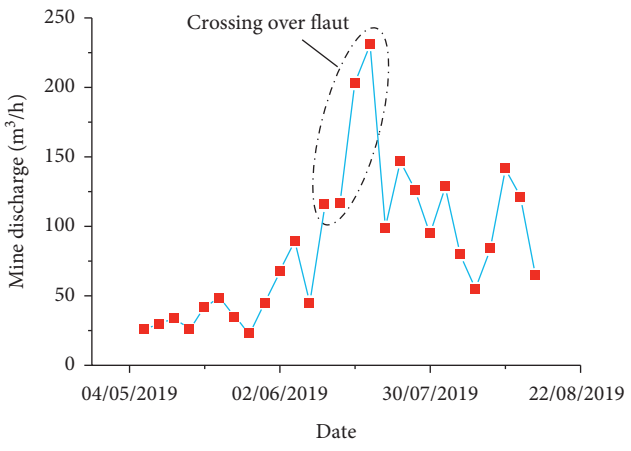

Figure 10: Overview of water gushing in the working face.

through the fault, roof water inrush and slurry collapse events occurred several times in the 13–24 m section of the working face, and the roof of the working face collapsed. Each water inrush accident generated an inflow of 132 m^3/h, accompanied by a gap at the support (i.e., the 2# water inrush point). The whole water inrush process was uniform before crossing the fault and surged after the fault. Combined with the above numerical analysis, it could be concluded that at the early stage of uniform water inrush, the surrounding rock was broken due to its proximity to the structural area, tectonic stress, and mining pressure, but the surrounding rock of the working face did not produce a plastic zone connected with the aquifer, resulting in a small amount of consistent water seepage. Ten meters passed the fault, the sudden jump phenomenon occurred in the water-conducting fracture zone, and karst water quickly gushed out of the working face, resulting in a sudden surge in water. At 30 m after the fault, frequent and notable water gushing occurred due to the formation of a high-stress water pressure concentration area in the working face, resulting in multiple water gushing events accompanied by slurry collapse, which is consistent with the evolution trend of the roof fracture zone in the numerical simulations.

In summary, the key stratum exerts a good control effect on the stability of the roof of the surrounding rock. In the absence of structural influence, the development height of the fracture zone is 25 m, and no water inrush accidents occur. Later, due to the influence of faults, the control effect of key strata is weakened, the height of the fracture zone increases to 60 m, and the water inflow increases greatly. Therefore, it necessary to prospect the geological structure of working face in advance. In view of the situation that the working face encounters faults, special mining scheme should be formulated to reduce the stress concentration near the fault and prevent the occurrence of water inrush accident.

6. Conclusion

(1) Through a geological survey, it was found that there is a fault zone in the east of mining face 5914. Based

on the key stratum theory, the fine sandstone layer above the no. 9 coal seam was identified as the key stratum, and the water hazard source was determined as the Changxing Formation aquifer via hydrochemistry.

(2) The numerical simulation results of RFPA-flow show that without the influence of faults, the AE events were evenly distributed within a small range in the deep surrounding rock due to the presence of key layers. With the tunneling of the working face, the shear stress concentration phenomenon appears below the key strata, and deformation occurred at the center of the roof. The fracture zone gradually formed a separation zone below the key stratum, and the final fracture height reached approximately 25 m.

(3) Under the action of fault weakening, AE events at the early stage converged at the hinge point of the fault and key stratum and then rapidly expanded both horizontally and longitudinally. The number of AE events surged to 1150, and the observed fissures were consistent with the AE phenomenon. Moreover, the sudden jump phenomenon occurred vertically, after which the fissures quickly penetrated the aquifer and formed a water-conducting fissure zone. The height reached 60 m, which is 2~3 times as high as that in the case of no faults.

(4) In the process of working face tunneling, the hydraulic gradient curve is characterized by small amplitude and uniform downward extension due to the existence of key strata. However, when the working face is driven to the affected area of the fault, the hydraulic gradient curve extends to the working face in a large area, which increase the risk of water damage accidents in the later period.

Data Availability

Some or all data, models, or codes generated or used during the study are available from the corresponding author upon request.

Conflicts of Interest

The authors announced that there are no conflicts of interest regarding the publication of this paper.

Acknowledgments

This work was supported by the National Natural Science Foundation of China (No. 52164006), Guizhou Provincial Science and Technology Projects (No. [2022]248), the National Natural Science Foundation for Young Teachers of Guizhou University (No. [2020] 81), and Risk Assessment of Water Hazard in No. 13 Coal Seam Floor in No. 2 Mining Area of Longfeng Coal Mine and Research on Water Prevention and Control Measures (No. K21-0111-025).

References

[1] W. J. B. Sun, Y. J. Zuo, S. Y. Wang et al., "Pore structures of shale cores in different tectonic locations in the complex tectonic region: a case study of the Niutitang Formation in Northern Guizhou, Southwest China," *Journal of Natural Gas Science and Engineering*, vol. 80, Article ID 103398.

[2] X. G. Cheng, W. Qiao, G. F. Li, and Z. Yu, "Risk assessment of roof water disaster due to multi-seam mining at Wulunshan Coal Mine in China," *Arabian Journal of Geosciences*, vol. 14, no. 12, p. 1116, 2021.

[3] B. Kong, Z. Y. Cao, T. Sun, C. Qi, and y. Zhang, "Safety Hazards in Coal Mines of Guizhou China during 2011–2020," *Safety Science*, vol. 145, Article ID 105493, 2022.

[4] S. H. Prassetyo and M. Gutierrez, "Effect of transient coupled hydro-mechanical response on the longitudinal displacement profile of deep tunnels in saturated ground," *Tunnelling and Underground Space Technology*, vol. 75, pp. 11–20, 2018.

[5] F. Song, A. Rodriguez-Dono, and S. Olivella, "Hydro-mechanical modelling and analysis of multi-stage tunnel excavations using a smoothed excavation method," *Computers and Geotechnics*, vol. 135, Article ID 104150.

[6] W. J. Yu, W. J. Wang, G. S. Wu, X. Yu, and W. Peng, "Three zones and support technique for large section incline shaft crossing goaf," *Geotechnical & Geological Engineering*, vol. 35, no. 5, pp. 1921–1931, 2017.

[7] L. Q. Shi, X. Y. Qu, X. G. Yu et al., "Theory and practice on the division of the "water pressure-free zone" in a mining coal seam floor," *Arabian Journal of Geosciences*, vol. 13, no. 20, p. 1079, 2020.

[8] J. L. Xie and J. L. Xu, "Effect of key stratum on the mining abutment pressure of a coal seam," *Geosciences Journal*, vol. 21, no. 2, pp. 267–276, 2017.

[9] Y. P. Liang, B. Li, and Q. L. Zou, "Movement type of the first subordinate key stratum and its influence on strata behavior in the fully mechanized face with large mining height," *Arabian Journal of Geosciences*, vol. 12, no. 2, p. 31, 2019.

[10] B. Li, Y. P. Liang, and Q. L. Zou, "Determination of working resistance based on movement type of the first subordinate key stratum in a fully mechanized face with large mining height," *Energy Science & Engineering*, vol. 7, no. 3, pp. 777–798, 2019.

[11] H. D. Duan, S. Y. Zhu, S. W. Cao, and M. Zhang, "Safe feasibility of retaining sand-proof coal rock pillars in full-mechanized caving mining of extra-thick coal seam," *Arabian Journal of Geosciences*, vol. 14, no. 9, p. 778, 2021.

[12] T. J. Kuang, Z. Li, W. B. Zhu et al., "The impact of key strata movement on ground pressure behaviour in the Datong coalfield," *International Journal of Rock Mechanics and Mining Sciences*, vol. 119, pp. 193–204, 2019.

[13] T. Zhang, Q. Gan, Y. X. Zhao et al., "Investigations into mining-induced stress–fracture–seepage field coupling effect considering the response of key stratum and composite aquifer," *Rock Mechanics and Rock Engineering*, vol. 52, no. 10, pp. 4017–4031, 2019.

[14] J. Sun and X. X. Miao, "Water-isolating capacity of an inclined coal seam floor based on the theory of water-resistant key strata," *Mine Water and the Environment*, vol. 36, no. 2, pp. 310–322, 2017.

[15] Y. J. Zhou, M. P. Li, X. D. Xu, and M. Li, "A study on dual-load-zone model of overlying strata and evolution law of mining stress," *Computers, Materials & Continua*, vol. 58, no. 2, pp. 391–407, 2019.

[16] W. G. Du, J. Chai, D. D. Zhang, and W. Lei, "The study of water-resistant key strata stability detected by optic fiber sensing in shallow-buried coal seam," *International Journal of Rock Mechanics and Mining Sciences*, vol. 141, p. 104604.

[17] Z. H. Wu, M. T. Tang, Y. J. Zuo et al., "Acoustic Emission-Based Numerical Simulation of Tectonic Stress Field for Tectoclase Prediction in Shale Reservoirs of the Northern Guizhou Area, China," *Energy Geoscience*.

[18] W. J. Sun, W. F. Zhou, and J. Jiao, "Hydrogeological classification and water-inrush accidents in China's coal mines," *Mine Water and the Environment*, vol. 35, no. 2, pp. 214–220, 2016.

[19] J. J. Zhang, K. J. Xu, G. Reniers, and G. You, "Statistical analysis the characteristics of extraordinarily severe coal mine accidents (ESCMAs) in China from 1950 to 2018," *Process Safety and Environmental Protection*, vol. 133, pp. 332–340, 2020.

[20] J. H. Zhao, L. Bo, C. Juntao, and J. Ning, "Mechanism of seepage-stress fault water-inrush and grouting seal," *Arabian Journal of Geosciences*, vol. 13, no. 11, p. 404, 2020.

[21] Y. Wang, W. K. Feng, and C. H. Li, "On anisotropic fracture and energy evolution of marble subjected to triaxial fatigue cyclic-confining pressure unloading conditions," *International Journal of Fatigue*, vol. 134, p. 105524.

[22] Y. Wang, D. Q. Liu, J. Q. Han, C. Li, and H. Liu, "Effect of fatigue loading-confining stress unloading rate on marble mechanical behaviors: an insight into fracture evolution analyses," *Journal of Rock Mechanics and Geotechnical Engineering*, vol. 12, no. 6, pp. 1249–1262, 2020.

[23] W. B. Sun, Y. C. Xue, T. T. Li, and W. Liu, "Multi-field coupling of water inrush channel formation in a deep mine with a buried fault," *Mine Water and the Environment*, vol. 38, no. 3, pp. 528–535, 2019.

[24] H. Liu, Y. J. Zuo, Z. H. Wu et al., "Fractal analysis of mesoscale failure evolution and microstructure characterization for sandstone using DIP, SEM-EDS, and micro-CT," *International Journal of Geomechanics*, vol. 21, no. 9, 2021.

[25] H. Liu, L. L. Zheng, Y. J. Zuo et al., "Study on mesoscopic damage evolution characteristics of single joint sandstone based on micro-CT image and fractal theory," *Shock and Vibration*, pp. 1–18, Article ID 6547028, 2021.

[26] K. Ma, F. Z. Yuan, D. Y. Zhuang, Q. Li, and Z. Wang, "Study on rules of fault stress variation based on microseismic monitoring and numerical simulation at the working face in the dongjiahe coal mine," *Shock and Vibration*, pp. 1–12, 2019.

[27] X. Yu, K. Zhao, Q. Wang et al., "Relationship between movement laws of the overlaying strata and time space of the mined-out," *Geofluids*, 2020.

[28] L. Y. Zhang, Z. Q. Qu, Y. Chen et al., "Numerical simulation of hydro-force coupled crack progation," *Fresenius Environmental Bulletin*, vol. 28, pp. 4923–4934, 2019.

[29] J. N. Wang, W. T. Liu, and J. J. Shen, "Investigation on the fracturing permeability characteristics of cracked specimens and the formation mechanism of inrush channel from floor," *Shock and Vibration*, vol. 2021, pp. 1–12.

[30] J. L. Xu, W. Qin, and D. Y. Xuan, "Accumulative effect of overburden strata expansion induced by stress relief," *Journal of China Coal Society*, vol. 45, no. 1, pp. 35–43, 2020.

[31] X. Y. Qin, Y. H. Zhang, and Z. A. Huang, "Breaking mechanism and control technology of hard roof in deep and thin coal seam protective layer," *Journal of Central South University*, vol. 52, no. 11, pp. 4010–4020, 2021.

[32] X. X. Men, C. A. Tang, Z. Han, and T. Ma, "Numerical simulation to influence of perforation angle on fracture propagation under hydraulic fracturing," *Journal of Northeastern University*, vol. 34, no. 11, pp. 1638–1641, 2013.

[33] T. H. Yang, C. A. Tang, and W. C. Zhu, "Coupling analysis of seepage and stresses in rock failure process," *Chinese Journal of Geotechnical Engineering*, vol. 4, pp. 489–493, 2001.

[34] T. H. Yang, C. A. Tang, and H. Y. Liu, "Numerical model of the instability-failure process of the coal-bed floor due to confined water-inrush," *Journal of Geomechanics*, vol. 3, pp. 281–288, 2003.

[35] G. H. Zou, C. Zhang, and D. Tian, "Study on the formation mechanism of water conducting channel of overburden strata crossing fault Group in fully mechanized caving face," *Metal Mine*, vol. 5, pp. 65–70, 2021.

[36] K. Yang and S. Liu, "Rule of multi-key strata movement-fracture evolution-dynamics of gas emission in deep long distance lower protective layer mining," *Journal of Mining & Safety Engineering*, vol. 37, no. 5, pp. 991–1000, 2020.